

# CaBaFL: Asynchronous Federated Learning via Hierarchical Cache and Feature Balance

Zeke Xia

East China Normal University  
Shanghai, China

Ming Hu\*

Nanyang Technological University  
Singapore, Singapore  
hu.ming.work@gmail.com

Dengke Yan

East China Normal University  
Shanghai, China

Xiaofei Xie

Singapore Management University  
Singapore, Singapore

Tianlin Li

Nanyang Technological University  
Singapore, Singapore

Anran Li

Nanyang Technological University  
Singapore, Singapore

Junlong Zhou

Nanjing University of Science and  
Technology  
Nanjing, China

Mingsong Chen\*

East China Normal University  
Shanghai, China  
mschen@sei.ecnu.edu.cn

## Abstract

Federated Learning (FL) as a promising distributed machine learning paradigm has been widely adopted in Artificial Intelligence of Things (AIoT) applications. However, the efficiency and inference capability of FL is seriously limited due to the presence of stragglers and data imbalance across massive AIoT devices, respectively. To address the above challenges, we present a novel asynchronous FL approach named CaBaFL, which includes a hierarchical **C**ache-based aggregation mechanism and a feature **B**alance-guided device selection strategy. CaBaFL maintains multiple intermediate models simultaneously for local training. The hierarchical cache-based aggregation mechanism enables each intermediate model to be trained on multiple devices to align the training time and mitigate the straggler issue. In specific, each intermediate model is stored in a low-level cache for local training and when it is trained by sufficient local devices, it will be stored in a high-level cache for aggregation. To address the problem of imbalanced data, the feature balance-guided device selection strategy in CaBaFL adopts the activation distribution as a metric, which enables each intermediate model to be trained across devices with totally balanced data distributions before aggregation. Experimental results show that compared with the state-of-the-art FL methods, CaBaFL achieves up to 9.26X training acceleration and 19.71% accuracy improvements.

## 1 Introduction

With the prosperity of Artificial Intelligence (AI) and Internet of Things (IoT), Artificial Intelligence of Things (AIoT) is becoming the main-stream paradigm for the design of large-scale distributed systems [9, 38]. Federated Learning (FL) [10, 21, 27, 44] as an important distributed machine

learning paradigm has been widely used in AIoT-based applications, e.g., mobile edge computing [35], healthcare systems [24, 25], and autonomous driving [31, 43]. Typically, AIoT-based FL consists of a central server and a large number of AIoT devices. The cloud server maintains a global model and dispatches it to multiple AIoT devices for training. Each AIoT device trains its received global model using its local data and then uploads the local model to the server. By aggregating all the local models, the server can achieve collaboratively global model training without leaking the raw data of any devices.

However, due to the heterogeneity of devices and data, AIoT-based FL still encounters two main challenges. The first challenge is the straggler problem. The heterogeneous nature of AIoT devices (e.g., varying computing and wireless network communication capacities), can result in significant differences in the training time for each device [23, 40]. Aggregating all the local models, including those from devices with poor computation capabilities, can lead to longer training time. The second challenge is that the data among AIoT devices are not independent-and-identically-distributed (non-IID) [32]. Such a data imbalance issue among AIoT devices can lead to the problem of “weight divergence” [13] and results in the inference accuracy degradation of the global model [15, 16, 20, 29]. To address the above challenges, the existing solutions can be mainly classified into three schemes, i.e., synchronous [14, 22, 45], asynchronous [4, 33, 37], and semi-asynchronous [11, 26, 36, 42]. In synchronous FL methods [27], the cloud server generates the global model after receiving all the local models. The non-IID problem could be alleviated with some well-designed training and client selection strategies [3, 5, 12, 22], while the straggler problems cannot be well addressed. Asynchronous FL methods [37] directly aggregate the uploaded local model to update the global model without waiting for other local models. By a timeout strategy, asynchronous FL methods could discard

\*Corresponding authors

stragglers, thereby avoiding the inefficient update in the global model. However, non-IID scenarios still seriously limit the performance of existing asynchronous FL methods. Semi-asynchronous FL methods [26, 36] maintain a buffer to store uploaded local models, when the stored models reach a certain number, the server performs an aggregation operation and clears the buffer. Although semi-asynchronous FL methods can alleviate the straggler problems, they still encounter the problems of non-IID data. Due to adopting different training mechanisms, synchronous methods are often difficult to combine directly with asynchronous methods. *Therefore, how to ensure performance in scenarios of data imbalance while solving the straggler problem is a huge challenge.*

To address both challenges of the straggler and data imbalance, this paper presents a novel asynchronous FL approach named CaBaFL, which maintains a hierarchical Cache structure to allow each intermediate model to be asynchronously trained by multiple clients before aggregation and uses a feature **B**alance-guided client selection strategy to enable each model to be eventually trained by totally balance data. To address the challenge of stragglers, we use a hierarchical cache-based aggregation mechanism to achieve asynchronous training. Specifically, we use multiple intermediate models for local training and to guarantee the number of activated devices, we enable each intermediate model participant in the aggregation after multiple times local training. To facilitate the asynchronous aggregation, each intermediate model is stored in the low-level cache named L2 cache. When trained with sufficient devices, a model can be stored in the high-level cache named L1 cache. While a certain number of devices trains a model, it will be updated with the global model aggregated with all the models in the L1 cache. Based on our asynchronous mechanism, the feature balance-guided device selection strategy wisely selects a device for each intermediate model that aims to let the total data used to train the model be balanced before aggregation. However, gaining direct access to the data distribution of each device could potentially compromise users’ privacy. To address this concern, we are inspired by the observation that the middle-layer features strongly reflect the underlying data distribution (more details are in Section 3) and propose a method to select devices based on their middle-layer activation patterns. This paper has three major contributions:

- We present a novel asynchronous FL framework named CaBaFL, which enables multiple intermediate models for collaborative training asynchronously using a hierarchical cache-based aggregation mechanism.
- We present a feature balance-guided device selection strategy to wisely select devices according to the activation distribution to make each intermediate model be trained with totally balanced data, which alleviates the performance deterioration caused by data imbalance.
- We conduct experiments on both well-known datasets and models to show the effectiveness of our approach for both IID and non-IID scenarios.

The rest of this paper is organized as follows. After the introduction to related work on asynchronous FL in Section 2, Section 3 presents the motivation of our method. Section 4 presents the details of our CaBaFL approach. Section 5 evaluates the effectiveness of our approach and conducts a comparative analysis with state-of-the-art (SOTA) FL methods. In Section 6, we explore some of the topics and limitations of CaBaFL that deserve discussion and future research. Finally, Section 7 concludes the paper.

## 2 Preliminary and Related Work

### 2.1 Preliminary of Federated Learning.

In general, a Federated Learning system consists of one cloud server and multiple dispersed clients. In each round of training in federated learning, the cloud server first selects a subset of devices to distribute the global model. After receiving the model, the devices conduct local training and upload the model to the cloud server. Finally, the cloud server aggregates the received models and obtains a new global model. The learning objective of FL is to minimize the loss function over the collection of training data at  $N$  clients, i.e.,

$$\min_w F(w) = \sum_{k=1}^N \frac{|D_k|}{|D|} F_k(w), \quad (1)$$

where  $N$  is the number of clients that participate in local training,  $w$  is the global model parameters,  $D_k$  is the  $k^{th}$  client and  $|D_k|$  represents the training data size on  $D_k$ ,  $F_k(w) = \frac{1}{|D_k|} \sum_{j \in D_k} f_j(w)$  is the loss empirical objective over the data samples at client  $k$ .

### 2.2 Related Work.

Asynchronous FL has a natural advantage in solving the straggler effect, where the server can aggregate without waiting for stragglers. [37] develop a FedASync algorithm, which combines a function of staleness with asynchronous update protocol. In FedASync, whenever a model is uploaded, the server directly aggregates it. Although FedASync can solve the straggler problem, some stragglers may become stale models, thereby reducing the accuracy of the global model. In addition, the client in FedASync will send a large number of models to the server, causing a lot of communication overhead. In terms of reducing data transmission, Wu et al. [36] propose a SAFA protocol, in which asynchronous clients continuously perform local updates until the difference between the local update version and the global model version reaches tolerance. Although SAFA considers model staleness, the server needs to wait for the asynchronous clients. Moreover, SAFA needs to maintain a bigger buffer compared to FL, which can cause more memory costs and thus lead to high complexity and low scalability. Similarly,

Ma et al. [26] set a model buffer for model aggregation to achieve semi-asynchronous FL and dynamically adjust the learning rate and local training epochs to mitigate the impact of stragglers and data heterogeneity.

However, none of the above methods can solve the problem of data heterogeneity well. To solve the problem of data heterogeneity, Zhou et al. [46] propose a WKAF protocol, which leverages the stale models of stragglers by maintaining a globally unbiased gradient and mitigates the impact of data heterogeneity through gradient clipping. Moreover, WKAF uses a two-stage strategy to accelerate training. In the early stage of training, the server does not perform gradient clipping to speed up training. Gradient clipping is only performed after a certain number of rounds of training. In [8], Hu et al. use the semi-asynchronous FL mechanism. In this method, a buffer is maintained in the server to store the model sent by clients. The server attempts to alleviate the impact of data heterogeneity by minimizing the variance of hard labels in the buffer. However, this method requires the clients to send the hard labels to the server. Unfortunately, in real-world scenarios, hard labels of data often contain sensitive information and cannot be obtained by the server.

To the best of our knowledge, CaBaFL is the first attempt that employs collaborative training and feature balance-guided device selection strategy in asynchronous federated learning to enhance both model accuracy and training stability.

### 3 Motivation

#### 3.1 Intuition of Our Asynchronous Mechanism

Figure 1 presents the intuition of our asynchronous FL mechanism. A conventional FL framework cannot maintain the activation of all three devices due to the presence of stragglers, as depicted in Figure 1(a). To ensure a sufficient number of active devices and reduce the overall training time, an optimal solution is to enable the model to participate in the aggregation process after training on multiple devices. Figure 1(b) illustrates the desired scenario, where a device is activated for local training immediately upon receiving a local model, and aggregation occurs after multiple rounds of local training. This approach allows most of the time to have three devices actively engaged in training. Furthermore, the synchronous aggregation mechanism has to wait for all local training to be completed, resulting in wasted time [19, 28, 39, 41]. To overcome these problems, CaBaFL introduces an asynchronous training approach that enables multiple clients to participate concurrently. Additionally, it incorporates an asynchronous aggregation mechanism to enhance overall efficiency. Please refer to Section 4 for more details.

#### 3.2 Connection between Data and Activation Distributions

To mitigate the challenge posed by data imbalance, our objective is to carefully choose devices for each intermediate model and ensure that the total data used for training the model is balanced before aggregation. Accomplishing this task necessitates having knowledge of the data distribution associated with each device. Due to the risk of privacy leakage, it is difficult for the server to obtain the data distribution of each device directly. Therefore, selecting an easily obtainable metric that does not compromise privacy to guide device selection, which ensures that each intermediate model is trained by balanced data is a key challenge for our asynchronous FL approach in dealing with the non-IID problem. We have made the following important observations that demonstrate the ability of middle-layer activation patterns to reflect the input data distribution of each device. Moreover, we have found that the middle-layer activation patterns can provide a more granular representation of the input data distribution than relying solely on input data labels. These observations motivate us to select devices based on their middle-layer activation patterns.

**Observation 1.** *To explore the connection between the activation distribution with the data distribution, we divide the CIFAR-10 dataset into 6 sub-datasets (i.e.,  $D_0 - D_5$ ), in which the data in  $D_0$  is balanced, i.e., IID, and the other five data are divided according to the Dirichlet distribution [7]  $\text{Dir}(\beta)$ , where a small value of  $\beta$  indicates a more seriously data imbalance among sub-datasets. We select ResNet-18 for model training and computing the activation distribution of a specific layer on the whole CIFAR-10 dataset and 6 sub-datasets respectively.*

Figures 2(a)-(c) present the cosine similarities of the activation distribution using the whole CIFAR-10 dataset with that using 6 sub-datasets, with  $\beta = 0.1, 0.5, \text{ and } 1.0$ , respectively. We can observe that the  $D_0$  achieves the highest cosine similarity and the sub-datasets divided with a smaller  $\beta$  achieves lower cosine similarity. Therefore, if the data distribution of a sub-dataset is more similar to that of the whole dataset, it achieves a higher cosine similarity of their activation distribution. Figures 2(d)-(f) present the cosine similarities of the activation distribution using the CIFAR-10 dataset with that using the combinations of 5 imbalance sub-datasets. Note that since the data in CIFAR-10 dataset and  $D_0$  is balanced, data of the combination of all the 5 imbalance sub-datasets is balanced. From Figures 2(d)-(f), we can observe that with the data distribution of the combination dataset close to the whole dataset, the cosine similarity of their activation distribution becomes higher. Because the activation amount is obtained by counting the number of times the neuron is activated, the activation amount of the combination dataset is equal to the sum of that of all the combined datasets.

**Observation 2.** *Due to the preference difference of devices, even if they have the same data label, the features of their data*

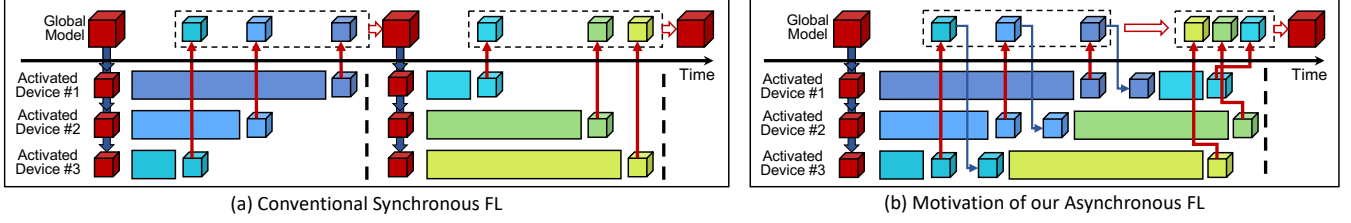


Figure 1. A motivating example of our asynchronous FL method with three activated devices.

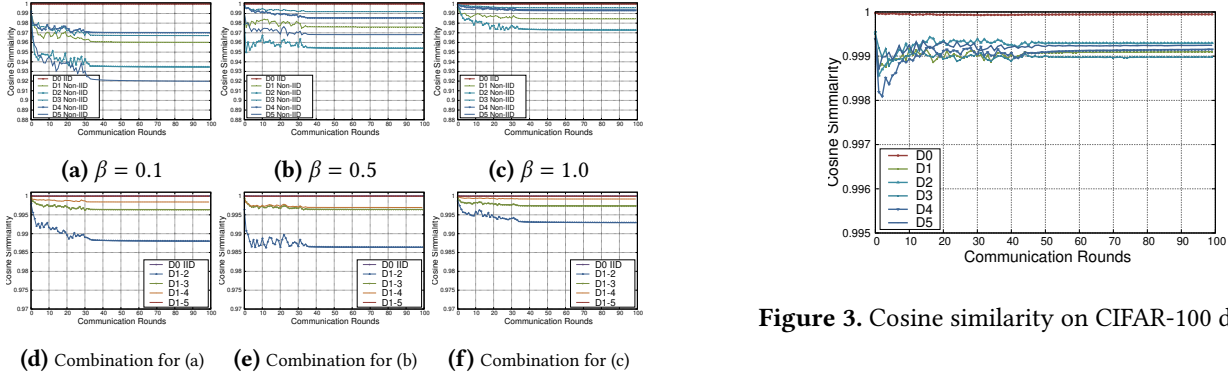


Figure 2. Cosine similarity of activation distribution.

may be quite different. For example, for the “Dog” category, some users prefer Husky dogs, and some users prefer Teddy dogs. Therefore, the data category distribution sometimes ignores the differences between the same category data.

To explore whether the differences between the same category data can lead to different activation distributions, we select the CIFAR-100 dataset, which contains 100 fine-grained and 20 coarse-grained classifications. We divide the CIFAR-100 dataset into six sub-datasets (i.e.,  $D_0 - D_5$ ), in which the data in  $D_0$  is balanced on fine-grained classifications and the other five data are balanced on course-gained classifications but imbalanced on fine-grained classifications. We conduct model training on the task of the coarse-grained classification and computing the activation distribution of a specific layer on the whole CIFAR-100 dataset and six sub-datasets, respectively. Figure 3 presents the cosine similarities of the activation distribution using the CIFAR-100 dataset with 6 sub-datasets. We can observe that  $D_0$  can achieve the highest cosine similarity and the difference in data with the same category can result in a decrease in the similarity of activation distribution. Therefore, compared to the data distribution, the activation distribution can express the differences between data in a more fine-grained manner.

Based on the above observations, in our approach, we use activation distribution as a metric to guide the server to select devices to make each intermediate model trained by more balanced data.

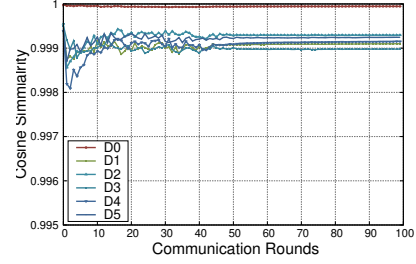


Figure 3. Cosine similarity on CIFAR-100 dataset.

## 4 Our CaBaFL Approach

### 4.1 Overview

Figure 4 illustrates the framework and workflow of our CaBaFL approach, which consists of a central cloud server and multiple AIoT devices, i.e.,  $D_1 - D_N$ , where the cloud server includes two crucial components, i.e., a hierarchical cache-based model aggregation controller and a feature balance-guided device selector, respectively. The hierarchical cache-based model aggregation controller performs the model aggregation and updating according to the number of training times. The feature balance-guided device selector chooses clients for local training according to the cosine similarity between the feature of the model in the L2 cache and the global feature. Note that, according to the observations in Section 3, we select the activation of a specific layer as the metric to calculate the feature. In specific, we specify a layer  $l$  of a specific model  $m$ . The feature of a device is the activation amount of the  $l$  using the raw data of the device as input. The feature of an intermediate model is the activation amount of the  $l$  using all the data used to train it as input after its latest update. For example, assume that an intermediate model  $m_i$  is trained by devices  $D_i$  and  $D_j$ , its feature can be calculated with  $f_{m_i} = f_{D_i} + f_{D_j}$ . The global feature is the sum of all the device features. Assume there are  $N$  devices, the global feature can be calculated with  $f_g = \sum_{i=1}^N f_{D_i}$ .

As shown in Figure 4, the hierarchical cache-based model aggregation controller consists of a 2-level cache structure to store intermediate models and a cache update controller to control model updating in L1 cache. The feature balance-guided device selector consists of a model feature cache and a device feature cache, where the model feature cache records

the feature of each intermediate model and the device feature cache records the global feature and features of each device. When an intermediate model completes a time of local training, the device selector updates its feature by adding the feature of its latest dispatched device to its original feature.

In addition, CaBaFL periodically broadcasts the global model to all devices to collect their features. Upon receiving the global model, each device calculates the device feature using its raw data. After the feature collection, the server updates the device feature cache and model feature cache. Note that the feature collection process operates asynchronously with the FL training process.

As shown in Figure 4, the workflow of the FL training process for each intermediate model in CaBaFL includes five steps as follows.

- **Step 1 (Device Selection):** For an intermediate model, the device selector selects a device according to the feature and training times of the intermediate model and the features of candidate devices.
- **Step 2 (Model Dispatching):** The cloud server dispatches the intermediate model to the selected device for local training.
- **Step 3 (Model Uploading):** The device uploads the model to the cloud server after local training is completed.
- **Step 4 (Cache Update):** The cache update controller stores the received model in the L2 cache and decides if it updates the model to the L1 cache according to its training times and features.
- **Step 5 (Cache Aggregation):** If an intermediate model reaches the specified training times, the cloud server aggregates all the models in the L1 cache to generate a new global model and update the intermediate model using the global model.

In our approach, steps 1-5 will be repeated until the time threshold is reached. Note that since in the whole training process, none of the intermediate models need to wait for other intermediate models, in other word, all the intermediate models are trained asynchronously.

## 4.2 CaBaFL Implementation

Algorithm 1 presents the implementation of our CaBaFL approach. Assume that there are at most  $K$  activated clients participating in local training at the same time. Line 1 initializes all the caches. Note that the size of the L1 and L2 cache is  $K$  intermediate models. Lines 3-20 present the FL training process of models in the 2-level cache, where the “for” loop is a parallel loop. Line 5 represents that the model  $m_i$  is uploaded to the L2 cache after training on the device  $D_j$ . Line 6 represents the training times of  $m_i$  plus one. In Lines 7-11, the server updates  $m_i^{L1}$  using the eligible  $m_i$ . In Lines 8-10, the server updates the feature  $f_{m_i^{L1}}$  and the training data size for  $m_i^{L1}$  after the L1 cache is updated. Lines 12-17 present the

details of the model aggregation process. In Line 12, model aggregation is triggered when  $c_i$ , the training times of  $m_i$ , achieves  $k$ . In Line 13, the server aggregates models in the L1 cache to obtain a new global model  $m_{glb}$ . In Lines 14-16, the server replaces  $m_i$  and  $m_i^{L1}$  with the  $m_{glb}$  and reset the training times and model feature of  $m_i$ . In Line 18, the function  $DevSel()$  selects a device  $D_j$  for  $m_i$  to conduct model dispatching.

---

### Algorithm 1 Implementation of CaBaFL

---

**Input:**  $f_g$ , the global feature;  $f_D$ , the features of devices.

**Output:**  $m_{glb}$ , the global model;

**CaBaFL**( $f_g, f_D$ )

```

1: Initialize the caches.
2: /* Parallel for */
3: for  $i = 1, \dots, K$  do
4:   while  $t < T$  do
5:      $m_i \leftarrow LocalTrain(D_j, m_i)$ ;
6:      $c_i \leftarrow c_i + 1$ 
7:     if  $c_i > \frac{k}{2}$  or  $\frac{index(sim_i)}{len(sims)} > \gamma$  then
8:        $m_i^{L1} \leftarrow m_i$ ;
9:        $f_{m_i^{L1}} \leftarrow f_{m_i}$ ;
10:       $DS_i^{L1} \leftarrow DS_i$ ;
11:     end if
12:     if  $c_i = k$  then
13:        $m_{glb} \leftarrow Aggr(m^{L1}, CS, DS^{L1})$ ;
14:        $m_i^{L1} \leftarrow m_i \leftarrow m_{glb}$ ;
15:        $c_i \leftarrow 0$ ;
16:        $f_{m_i} \leftarrow null$ ;
17:     end if
18:      $D_j \leftarrow DevSel(f_g, f_{m_i}, f, DS, S, c_i)$ ;
19:   end while
20: end for
21: return  $m_{glb}$ 

```

---

### 4.2.1 Hierarchical Cache-based Asynchronous Aggregation. Hierarchical cache updating.

CaBaFL maintains a 2-level cache in the cloud server to screen models in the L2 cache. When a model completes local training and is uploaded to the cloud server, the cloud server first saves the model in the L2 cache. Then the server calculate the cosine similarity  $sim_i$  between the model features  $f_{m_i}$  and the global features  $f_g$ :  $sim_i = \text{cossim}(f_g, f_{m_i}) = \frac{f_g \cdot f_{m_i}}{\|f_g\| \|f_{m_i}\|}$ . If  $sim_i$  is low, aggregating these models has a negative impact on the performance of the global model. To perform effective model screening, the cloud server maintains a sorted list  $sims$ , which records the similarity between the features of all models trained and  $f_g$ . The server adds  $sim_i$  to  $sims$ .  $m_i^{L1}$  will be updated to  $m_i$ , if  $\frac{index(sim_i)}{len(sims)} > \gamma$ , where  $index(sim_i)$  represents the index of  $sim_i$  in  $sims$  and  $len(sims)$  represents the length of  $sims$ . In addition, if the number of model training times exceeds half of the specified times, i.e.  $c_i > \frac{k}{2}$ , the

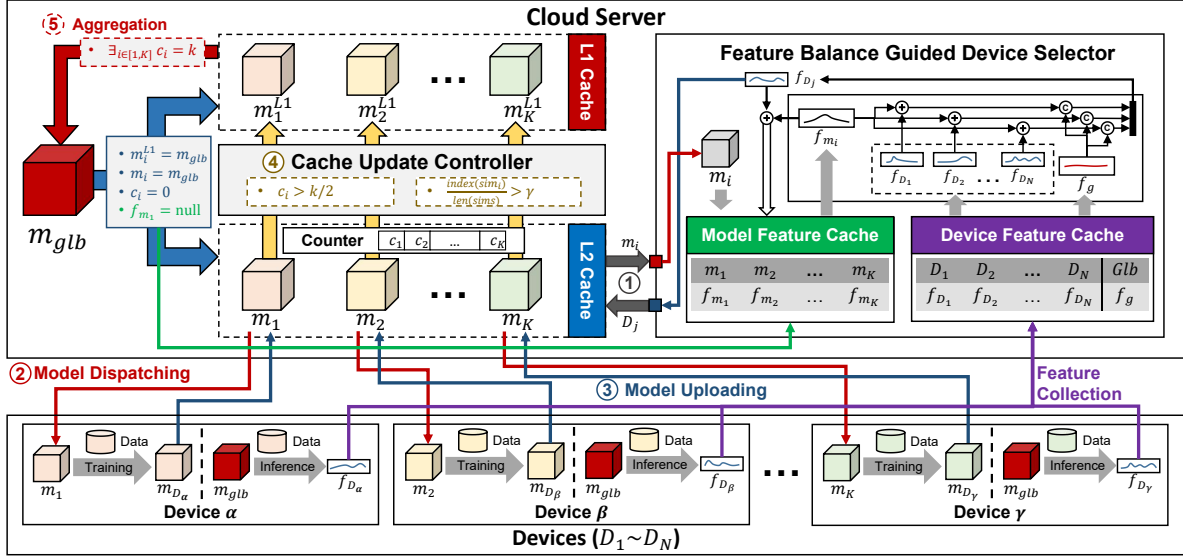


Figure 4. Framework and workflow of CaBaFL.

cloud server will also update  $m_i^{L1}$  to  $m_i$  because the model has learned enough knowledge to participate in model aggregation.

**Model aggregation strategy ( $Aggr(\cdot)$ ).** In cache aggregation, our approach calculates a weight for the model in the L1 cache based on the training data size and the similarity between the model features and global features. The aggregation process is shown as follows:

$$Aggregation(m^{L1}, CS, DS^{L1}) = \frac{\sum_{i=1}^K m_i^{L1} \times \frac{(DS_i^{L1})^\alpha}{1-CS_i}}{\sum_{i=1}^K \frac{(DS_i^{L1})^\alpha}{1-CS_i}}, \quad (2)$$

where  $m_i^{L1}$  represents the model in L1 cache,  $DS_i^{L1}$  represents the size of training data of  $m_i^{L1}$ ,  $CS_i$  represents the similarities between the features of the model in L1 cache  $f_{m_i^{L1}}$  and the global features  $f_g$ ,  $K$  represents the size of the cache, and  $\alpha$  is a hyperparameter that is less than 1.

To calculate the weight, we first calculate the model weights based on the model's training data size. Due to the possibility of different numbers of training times of the model in the L1 cache, there may be significant differences in the training data size of the model. Therefore, if we directly use the training data size as the weight, it may harm the performance of the global model when data heterogeneity is high. Therefore, we use the hyperparameter  $\alpha$  to mitigate this effect. After that, we calculate the weights based on the similarity  $CS_i = \text{cossim}(f_g, f_{m_i^{L1}})$ . The higher the  $CS_i$ , the more balanced the model features are, and the higher the weight is assigned to the model. Since the similarity between models is very close to 1, to achieve small differences between them, we use  $1 - CS_i$  to amplify these differences.

**4.2.2 Feature Balance Guided Device Selection.** Algorithm 2 presents the device selection strategy of CaBaFL. When selecting devices, greedily choosing the device with the greatest similarity between model features and global features can lead to fairness issues by causing some devices to be selected repeatedly while others are rarely selected. Therefore, CaBaFL sets a hyperparameter  $\sigma$ . When the variance of the number of times devices are selected exceeds  $\sigma$ , the server selects devices from those idle devices with the fewest selections; otherwise, the selection range is all idle devices (Lines 1-4). If the model has just started a new training round, i.e.,  $c_i = 0$ , the server randomly selects a device for the model to start a new training round (Lines 5-6). Otherwise, for each device  $D_j$ , CaBaFL calculates the cosine similarity  $w_1$  between the model features and the global features when  $D_j$  is selected (Line 10). CaBaFL also considers balancing the training data size of the model in the L2 cache when selecting devices. Since the training time of a device is often directly proportional to the size of its data, balancing the model training data size can indirectly balance training time between models in the L2 cache, thereby alleviating the adverse effects caused by stragglers. So CaBaFL calculates the variance of the training data size of the model in the L2 cache when  $D_j$  is selected (Lines 11-13), where  $|D_j|$  represents the training data size on  $D_j$ .  $w_1$  is then subtracted by the variance to obtain the weight of the device (Line 14), and the device with the highest weight is selected for model dispatching (Line 16). Finally, CaBaFL updates  $S_{res}$ ,  $f_{m_i}$  and  $DS_i$  (Lines 17-19).

**Table 1.** Comparison of test accuracy for both IID and non-IID scenarios.

Dataset	Model	Heterogeneity Settings	Test Accuracy (%)						
			FedAvg [27]	FedProx [22]	FedASync [37]	FedSA [26]	SAFA [36]	WKAFL [46]	CaBaFL
CIFAR-10	ResNet-18	$\beta = 0.1$	45.65 $\pm$ 3.52	45.57 $\pm$ 1.42	47.34 $\pm$ 0.72	47.26 $\pm$ 1.61	42.20 $\pm$ 2.63	40.86 $\pm$ 5.98	<b>55.46 <math>\pm</math> 0.67</b>
		$\beta = 0.5$	60.34 $\pm$ 0.37	58.66 $\pm$ 0.27	60.70 $\pm$ 0.28	60.59 $\pm$ 0.28	57.69 $\pm$ 0.71	67.84 $\pm$ 0.78	<b>69.31 <math>\pm</math> 0.18</b>
		$\beta = 1.0$	65.79 $\pm$ 0.34	63.55 $\pm$ 0.11	66.61 $\pm$ 0.22	65.11 $\pm$ 0.27	61.92 $\pm$ 0.44	71.19 $\pm$ 0.49	<b>72.84 <math>\pm</math> 0.36</b>
		IID	64.89 $\pm$ 0.17	63.78 $\pm$ 0.14	64.76 $\pm$ 0.10	64.98 $\pm$ 0.12	64.28 $\pm$ 0.16	73.50 $\pm$ 0.18	<b>74.83 <math>\pm</math> 0.07</b>
	CNN	$\beta = 0.1$	46.58 $\pm$ 1.29	46.59 $\pm$ 1.06	48.90 $\pm$ 0.68	48.58 $\pm$ 1.92	42.66 $\pm$ 2.23	41.03 $\pm$ 3.91	<b>52.92 <math>\pm</math> 0.62</b>
		$\beta = 0.5$	54.77 $\pm$ 0.60	54.33 $\pm$ 0.22	55.97 $\pm$ 0.66	55.44 $\pm$ 0.37	52.63 $\pm$ 1.30	50.25 $\pm$ 3.15	<b>57.89 <math>\pm</math> 0.59</b>
		$\beta = 1.0$	55.88 $\pm$ 0.53	55.72 $\pm$ 0.28	56.00 $\pm$ 0.31	56.45 $\pm$ 0.28	54.42 $\pm$ 1.02	53.88 $\pm$ 1.78	<b>58.58 <math>\pm</math> 0.72</b>
		IID	57.87 $\pm$ 0.19	57.76 $\pm$ 0.21	57.82 $\pm$ 0.09	57.94 $\pm$ 0.14	55.88 $\pm$ 0.17	58.15 $\pm$ 0.38	<b>61.75 <math>\pm</math> 0.30</b>
	VGG-16	$\beta = 0.1$	62.67 $\pm$ 5.15	63.31 $\pm$ 3.28	66.26 $\pm$ 1.24	65.26 $\pm$ 2.13	56.37 $\pm$ 3.95	55.09 $\pm$ 3.92	<b>70.68 <math>\pm</math> 1.49</b>
		$\beta = 0.5$	77.94 $\pm$ 0.46	77.15 $\pm$ 0.09	78.26 $\pm$ 0.20	78.02 $\pm$ 0.26	75.40 $\pm$ 0.87	78.78 $\pm$ 0.20	<b>82.36 <math>\pm</math> 0.25</b>
		$\beta = 1.0$	79.45 $\pm$ 0.41	78.58 $\pm$ 0.14	79.69 $\pm$ 0.17	78.64 $\pm$ 0.33	77.46 $\pm$ 0.75	80.19 $\pm$ 1.02	<b>83.81 <math>\pm</math> 0.27</b>
		IID	80.35 $\pm$ 0.05	79.22 $\pm$ 0.08	80.30 $\pm$ 0.06	80.42 $\pm$ 0.04	79.25 $\pm$ 0.14	82.89 $\pm$ 0.24	<b>85.12 <math>\pm</math> 0.05</b>
CIFAR-100	ResNet-18	$\beta = 0.1$	33.64 $\pm$ 0.52	33.24 $\pm$ 0.38	35.05 $\pm$ 0.41	33.61 $\pm$ 0.49	31.01 $\pm$ 1.04	27.65 $\pm$ 2.22	<b>37.77 <math>\pm</math> 0.35</b>
		$\beta = 0.5$	41.31 $\pm$ 0.19	40.08 $\pm$ 0.18	42.75 $\pm$ 0.37	41.96 $\pm$ 0.20	39.44 $\pm$ 0.44	44.78 $\pm$ 1.48	<b>47.30 <math>\pm</math> 0.28</b>
		$\beta = 1.0$	43.33 $\pm$ 0.19	41.76 $\pm$ 0.11	44.85 $\pm$ 0.23	42.75 $\pm$ 0.23	40.92 $\pm$ 0.23	47.41 $\pm$ 0.76	<b>48.10 <math>\pm</math> 0.44</b>
		IID	42.76 $\pm$ 0.09	42.63 $\pm$ 0.15	42.20 $\pm$ 0.18	43.18 $\pm$ 0.15	42.07 $\pm$ 0.16	49.10 $\pm$ 0.20	<b>49.64 <math>\pm</math> 0.06</b>
	CNN	$\beta = 0.1$	29.44 $\pm$ 0.65	30.64 $\pm$ 0.83	31.81 $\pm$ 0.57	30.52 $\pm$ 0.49	29.44 $\pm$ 1.44	19.18 $\pm$ 2.59	<b>33.22 <math>\pm</math> 0.48</b>
		$\beta = 0.5$	34.08 $\pm$ 0.64	34.73 $\pm$ 0.45	32.99 $\pm$ 0.30	34.70 $\pm$ 0.49	33.98 $\pm$ 0.95	28.88 $\pm$ 2.25	<b>36.44 <math>\pm</math> 0.39</b>
		$\beta = 1.0$	32.43 $\pm$ 0.48	32.74 $\pm$ 0.38	32.84 $\pm$ 0.27	34.27 $\pm$ 0.30	33.55 $\pm$ 0.35	31.35 $\pm$ 1.35	<b>37.31 <math>\pm</math> 0.49</b>
		IID	33.04 $\pm$ 0.24	33.55 $\pm$ 0.20	32.60 $\pm$ 0.22	33.23 $\pm$ 0.15	31.73 $\pm$ 0.37	32.99 $\pm$ 0.68	<b>36.88 <math>\pm</math> 0.33</b>
	VGG-16	$\beta = 0.1$	47.30 $\pm$ 1.27	47.29 $\pm$ 0.45	49.69 $\pm$ 0.68	46.91 $\pm$ 1.41	42.34 $\pm$ 1.66	30.82 $\pm$ 3.78	<b>50.53 <math>\pm</math> 0.49</b>
		$\beta = 0.5$	54.83 $\pm$ 0.59	53.80 $\pm$ 0.59	56.39 $\pm$ 0.47	54.55 $\pm$ 0.40	50.61 $\pm$ 0.66	53.08 $\pm$ 2.40	<b>57.37 <math>\pm</math> 0.37</b>
		$\beta = 1.0$	56.49 $\pm$ 0.21	54.50 $\pm$ 0.35	57.30 $\pm$ 0.35	55.24 $\pm$ 0.31	53.65 $\pm$ 0.40	56.71 $\pm$ 1.07	<b>59.53 <math>\pm</math> 0.17</b>
		IID	57.56 $\pm$ 0.05	56.30 $\pm$ 0.23	57.91 $\pm$ 0.13	56.39 $\pm$ 0.14	55.33 $\pm$ 0.24	61.16 $\pm$ 0.38	<b>64.96 <math>\pm</math> 0.04</b>
FEMNIST	ResNet-18	-	82.25 $\pm$ 0.43	81.57 $\pm$ 0.30	82.87 $\pm$ 0.35	82.07 $\pm$ 0.43	76.85 $\pm$ 0.35	74.68 $\pm$ 0.60	<b>84.08 <math>\pm</math> 0.17</b>
	CNN	-	81.29 $\pm$ 0.38	81.57 $\pm$ 0.29	82.68 $\pm$ 0.23	81.99 $\pm$ 0.46	76.82 $\pm$ 0.38	73.81 $\pm$ 0.58	<b>84.00 <math>\pm</math> 0.10</b>
	VGG-16	-	82.34 $\pm$ 0.38	81.38 $\pm$ 0.21	82.73 $\pm$ 0.26	82.00 $\pm$ 0.47	76.87 $\pm$ 0.39	74.62 $\pm$ 0.47	<b>84.30 <math>\pm</math> 0.13</b>

## 5 Performance Evaluation

### 5.1 Experimental Setup

To demonstrate the effectiveness of our approach, we implemented CaBaFL using the PyTorch framework [30] and conducted a comparative analysis with classical FedAvg [27] and five state-of-the-art FL methods (i.e., FedProx [22], FedASync [37], SAFA [36], FedSA [26], and WKAFL [46]), where FedProx is a synchronous method, FedASync is an asynchronous method and the latter three are semi-asynchronous method. For SAFA, FedSA, and WKAFL, we set the model buffer size to be half of the active device number. To ensure a fair comparison, we used an SGD optimizer with a learning rate of 0.01 and a momentum of 0.5 for all baselines and CaBaFL. Each client was trained locally for five epochs with a batch size of 50. All experimental results were obtained from a Ubuntu workstation equipped with an Intel i9 CPU, 64GB of memory, and an NVIDIA RTX 4090 GPU.

**Settings of Datasets and Models.** We conducted a comparative study of CaBaFL and baselines on three well-known datasets, i.e., CIFAR-10, CIFAR-100 [17], and FEMNIST [2]. To create the heterogeneity of device data for CIFAR-10 and CIFAR-100, we employed the Dirichlet distribution  $Dir(\beta)$

[7], where smaller values of  $\beta$  indicate greater data heterogeneity. As FEMNIST already possesses a non-IID distribution, we did not require the use of the Dirichlet distribution. Moreover, to show the pervasiveness of our approach, we conducted experiments on three well-known networks, i.e., CNN [18], ResNet-18 [6], and VGG-16 [34], respectively, which have different structures and depths.

**Settings of System Heterogeneity.** To simulate system heterogeneity, we simulated 100 devices with varying computing power and different network bandwidth. Firstly, we simulate different computing power based on the processing speed of true devices. Since the NVIDIA Jetson AGX Xavier device can be powered by different performance modes that can provide different computing power, we measured the processing speed under different performance modes and used it as the basis for simulating the computing power of our devices. To generate the simulated computing power, we used a Gaussian distribution with the mean and variance obtained from actual time consumption data of training models on Jetson AGX Xavier. Secondly, we simulated a fixed network bandwidth for each device to calculate the communication time required with the cloud server. In addition, we assume only 10% of devices can participate in training at the same time.

**Algorithm 2** The procedure of selecting device

**Input:** i)  $f_g$ , the global feature; ii)  $f$ , the features of devices; iii)  $DS$ , the data size of L2 cache; iv)  $S$ , selected times of devices; v)  $c_i$ , the training times of  $m_i$ ; vi)  $f_{m_i}$ , the feature of model  $m_i$ .

**Output:**  $D_j$ , selected device.

**DevSel**( $f_g, f, DS, S, c_i, f_{m_i}$ )

```

1:  $selectRange \leftarrow D^{idle}$ 
2: if  $\text{var}(S) > \sigma$  then
3:    $selectRange \leftarrow \{D_j \mid S_{D_j}^{idle} = \min(S^{idle})\}$ 
4: end if
5: if  $c_i = 0$  then
6:    $D_j \leftarrow$  select randomly from  $selectRange$ 
7: end if
8: return  $D_j$ 
9: for  $D_j$  in  $selectRange$  do
10:   $w_1 \leftarrow \text{cossim}(f_g, f_{m_i} + f_{D_j})$ 
11:   $DS'_i \leftarrow DS$ 
12:   $DS'_i \leftarrow DS'_i + |D_j|$ 
13:   $w_2 \leftarrow \text{var}(DS'_i)$ 
14:   $w_{D_j} \leftarrow w_1 - w_2$ 
15: end for
16:  $res \leftarrow \arg \max_{D_j} w_{D_j}$ 
17:  $S_{res} \leftarrow S_{res} + 1$ 
18:  $f_{m_i} \leftarrow f_{m_i} + f_{D_j}$ 
19:  $DS_i \leftarrow DS_i + |D_{res}|$ 
20: return  $res$ 

```

## 5.2 Performance Comparison

**5.2.1 Comparison of Accuracy.** Table 1 compares the test accuracy between CaBaFL and all the baselines on three datasets with different non-IID and IID settings using ResNet-18, CNN, and VGG-16 models. From Table 1, it can be observed that CaBaFL can achieve the highest test accuracy in all the scenarios regardless of model type, dataset type, and data heterogeneity. For example, CaBaFL improves test accuracy by 19.71% over WKaFL in CIFAR-100 dataset with VGG-16 model when  $\beta = 0.1$ . Figure 5 shows the learning curves of CaBaFL and all baseline methods on CIFAR-10 and ResNet-18. As an example of dataset CIFAR-10, when  $\beta = 0.1$  and the target accuracy is 45%, CaBaFL outperforms SAFA by 9.26X in terms of training time. Moreover, We can observe that CaBaFL achieves the highest accuracy and exhibits good stability in its learning curve.

Furthermore, we can find that our method can perform better than the baselines even in the IID scenario. This is mainly because in CaBaFL, a model can be trained on multiple devices before being aggregated, i.e., it can perform more times of stochastic gradient descent.

**5.2.2 Comparison of Communication Overhead.** Given a specific overall FL training objective regarding accuracy,

**Table 2.** Comparison of communication overhead.

Heter. Settings	Acc. (%)	Communication Overhead						
		FedAvg	FedProx	FedASync	FedSA	SAFA	WKaFL	CaBaFL
$\beta = 0.1$	40	1620	1620	<b>600</b>	1510	4700	7930	1360
	45	2300	2300	4220	2380	14640	7940	<b>2120</b>
$\beta = 0.5$	58	2760	2760	3160	3160	9550	2680	<b>1811</b>
	60	7860	-	11060	11040	-	3380	<b>2259</b>
$\beta = 1.0$	63	2920	5200	2580	4560	-	2960	<b>2085</b>
	65	7480	-	5760	10270	-	3270	<b>2279</b>
IID	63	1200	1220	<b>940</b>	1770	5800	1580	1593
	70	-	-	-	-	-	4010	<b>2441</b>

we compared the communication overhead caused by our method and all other baselines to achieve this objective. We conducted experiments on CIFAR-10 dataset using the ResNet-18 model, and the experimental results are shown in Table 2. Although collecting features periodically causes additional communication overhead, we can observe that in six out of eight cases, CaBaFL incurred the least communication overhead. For example, when  $\beta = 1.0$  and the target accuracy is 63%, CaBaFL outperforms FedASync by 0.81X in terms of communication overhead.

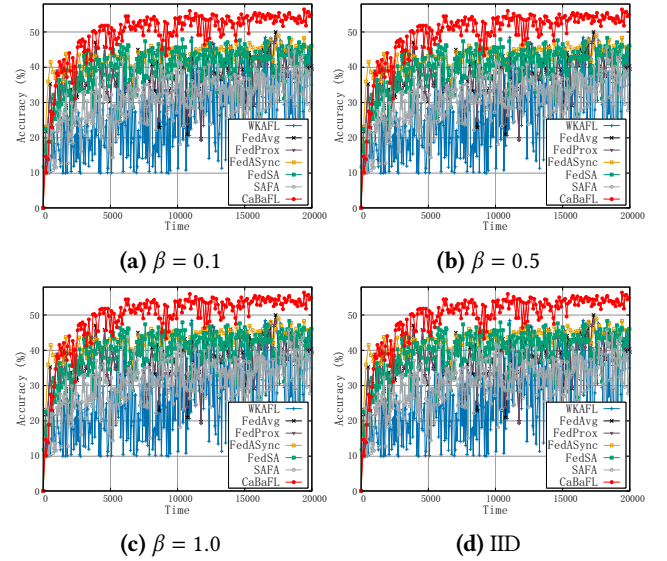


**Figure 5.** Learning curves of CaBaFL and all the baseline methods on CIFAR-10 with ResNet-18.

## 5.3 Impacts of Different Configuration

**5.3.1 Impacts of Different Features.** We investigated the impact of selecting features from different model layers on accuracy. Since ResNet-18 has 4 blocks, we performed pooling operations on the feature outputs of each block separately and used them as features when selecting the device. The feature dimensions of Blocks 1 to 4 are 64, 128, 256, and 512, respectively. Figure 6 shows all experiment results conducted on CIFAR-10 with IID distribution and Dirichlet distribution where  $\beta = 0.5$ . We can observe that selecting

the features from Block 4 performs the best. We can conclude that because of the highest dimensionality of Block 4, the features from Block 4 can represent data distribution in a more fine-grained manner, thus achieving the highest accuracy.

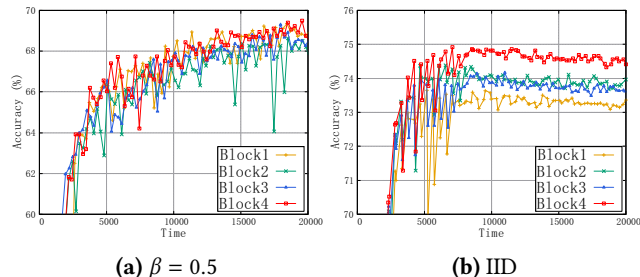


Figure 6. Impact of different features on test accuracy.

**5.3.2 Impacts of Different Number of Simultaneously Training Devices.** In the previous experiments, we assumed that 10% of the devices participate in the training at the same time. In this section, we investigate the impact of different numbers of devices trained simultaneously. We set up four different percentages of devices trained simultaneously, respectively 5%, 10%, 20%, and 50%, and conducted experiments using ResNet-18 on CIFAR-10 with Dirichlet distribution where  $\beta = 0.5$ . Figure 7 exhibits the experiment result. We can find that our method exhibits good scalability, and performs the best under different numbers of devices.

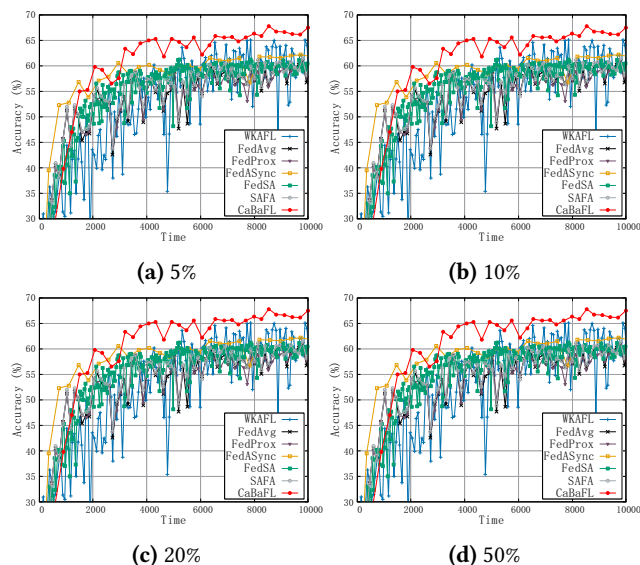


Figure 7. Learning curves for the cases with different numbers of simultaneously training clients.

**5.3.3 Impacts of Different Device Performance.** We conducted an experiment to assess the generalizability of CaBaFL in various AIoT environments. Our experiment took into account the impact of network conditions on delay and the varying computing capabilities of devices on local training time. To facilitate the evaluation, we combined the delay and local training time, assuming that their combinations adhere to Gaussian distributions. We consider five kinds of device conditions, i.e., excellent, high, medium, low, and critical as illustrated in Table 3. Based on Table 3, we consider four configurations that have different device compositions as shown in Table 4 to demonstrate the generalizability of our approach in different AIoT environments.

Table 3. Conditions for devices.

Quality	Excellent	High	Medium	Low	Critical
Device Settings	N(10,1)	N(15,2)	N(20,2)	N(30,3)	N(50,5)

Table 4. Configurations of different device compositions.

Config.	# of Clients				
	Excellent	High	Medium	Low	Critical
Config.1	40	30	10	10	10
Config.2	10	10	10	30	40
Config.3	10	20	40	20	10
Config.4	20	20	20	20	20

We conducted our experiments using the ResNet-18 model on the CIFAR-10 dataset with  $\beta = 0.1$ . Table 5 compares the accuracy between CaBaFL and baselines. We can find that CaBaFL can achieve the highest accuracy in all four cases and the accuracy of our method in different AIoT environments is more stable than the baselines.

Table 5. Comparison of test accuracy for different device configurations.

Configuration	Config.1	Config.2	Config.3	Config.4
	FedAvg	44.91 $\pm$ 2.63	44.78 $\pm$ 2.57	45.45 $\pm$ 2.83
FedProx	46.34 $\pm$ 2.55	44.59 $\pm$ 2.86	46.14 $\pm$ 3.11	43.79 $\pm$ 2.63
FedASync	50.31 $\pm$ 1.78	48.67 $\pm$ 1.65	50.12 $\pm$ 2.17	49.16 $\pm$ 1.47
FedSA	47.75 $\pm$ 2.32	46.32 $\pm$ 1.21	46.51 $\pm$ 2.54	47.04 $\pm$ 2.51
SAFA	41.68 $\pm$ 2.97	40.14 $\pm$ 2.51	41.32 $\pm$ 3.02	40.44 $\pm$ 3.88
WKaFL	49.06 $\pm$ 6.67	39.30 $\pm$ 6.65	46.79 $\pm$ 6.16	39.55 $\pm$ 5.12
CaBaFL	<b>56.96 <math>\pm</math> 0.58</b>	<b>56.06 <math>\pm</math> 0.50</b>	<b>56.13 <math>\pm</math> 0.54</b>	<b>56.74 <math>\pm</math> 0.60</b>

**5.3.4 Impacts of Different Model Training Times.** To investigate the impact of model training times  $k$ , we set up five different model training times, respectively 10, 15, 20, 25, and 30, and conducted experiments using ResNet-18 model on CIFAR-10 dataset with IID distribution. Figure 8 exhibits the experiment result. We can find that as the model training times  $k$  increase, the accuracy of the global model improves, but too high a number of model training times

leads to a decrease in global model accuracy and instability of the learning curve.

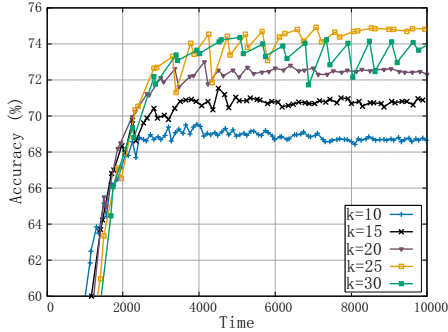


Figure 8. Impact of training times on test accuracy.

**5.3.5 Impacts of Task Type.** To demonstrate the generalizability of our approach on different types of tasks, we have applied our approach to the well-known NLP dataset Shakespeare [1] using the LSTM model. Figure 9 shows the experimental results. We can find that WKaFL, which performs well on image datasets, suffers a degradation on the NLP dataset. However, CaBaFL still can achieve the best accuracy which can prove the generalizability of CaBaFL on different tasks.

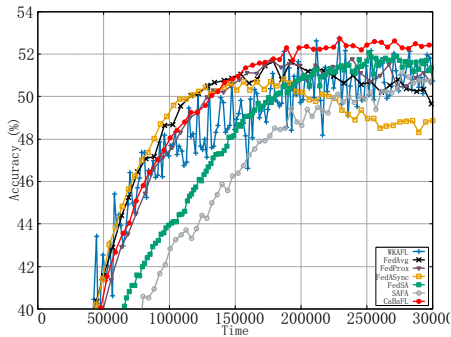


Figure 9. Learning curves of CaBaFL and all the baseline methods on Shakespeare with LSTM.

**5.3.6 Impacts of different feature collection cycles.** To investigate the impact of feature collection cycles, We assume that feature collection is performed after every  $m$  cache aggregation. We set  $m$  to be 1, 10, 20, 50, and 100, respectively, and conduct experiments on CIFAR-10 dataset and ResNet-18 model with both the IID distribution and the Dirichlet distribution (with  $\beta = 0.1$ ). Figure 10 exhibits the experiment results. From the results, we can find that both too-fast and too-slow feature collection cycles result in lower global model accuracy. In addition, a feature collection cycle that is too fast will significantly increase the communication overhead because the server needs to frequently send the global model to all devices for feature collection.

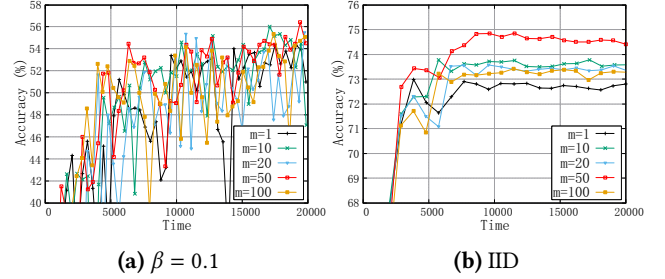


Figure 10. Impact of the feature collection cycle.

## 5.4 Ablation Study

**5.4.1 Key Components of CaBaFL.** To demonstrate the effectiveness of CaBaFL, we developed five variants of CaBaFL:

i) *Conf1* represents selecting devices based only on the similarity between model feature and global feature; ii) *Conf2* denotes selecting devices based only on data size; iii) *Conf3* indicates randomly selecting devices; iv) *Conf4* represents aggregating models in the L2 Cache, which means only L2 Cache is available in the server; and v) *Conf5* denotes averaging aggregation during model aggregation. We conducted experiments using the ResNet-18 model on CIFAR-10 with both non-IID and IID settings, and the results are presented in Table 6 and Figure 11. Table 6 shows that CaBaFL achieves the highest test accuracy among all six designs.

Table 6. Comparison of test accuracy among CaBaFL and its various variants.

Settings	Test Accuracy(%)			
	$\beta = 0.1$	$\beta = 0.5$	$\beta = 1.0$	IID
CaBaFL	55.46 $\pm$ 0.67	69.31 $\pm$ 0.18	72.84 $\pm$ 0.36	74.83 $\pm$ 0.07
Conf1	52.54 $\pm$ 0.95	69.05 $\pm$ 0.23	72.73 $\pm$ 0.23	73.99 $\pm$ 0.18
Conf2	54.16 $\pm$ 0.65	68.04 $\pm$ 0.20	71.59 $\pm$ 0.35	72.60 $\pm$ 0.18
Conf3	53.50 $\pm$ 1.23	69.16 $\pm$ 0.19	72.80 $\pm$ 0.34	72.67 $\pm$ 0.26
Conf4	53.29 $\pm$ 2.12	69.27 $\pm$ 0.42	72.49 $\pm$ 0.26	73.91 $\pm$ 0.09
Conf5	53.08 $\pm$ 0.49	68.30 $\pm$ 0.25	71.47 $\pm$ 0.12	72.99 $\pm$ 0.18

By comparing the performance of *Conf4* and CaBaFL, we observed that our 2-level cache structure significantly improves the stability of model training and enhances model accuracy in scenarios with high levels of data heterogeneity. By comparing the performance of *Conf5* and CaBaFL, we observed that our cache aggregation strategy significantly improves the accuracy of the model. Furthermore, by comparing the performance of *Conf1* to *Conf3* with that of CaBaFL, we observed that our feature balance-guided device selection strategy is effective in different scenarios of data heterogeneity. Especially under the extreme data heterogeneity condition where  $\beta = 0.1$ , our device selection strategy can significantly improve the accuracy of the global model compared to *Conf3*, which is random device selection.

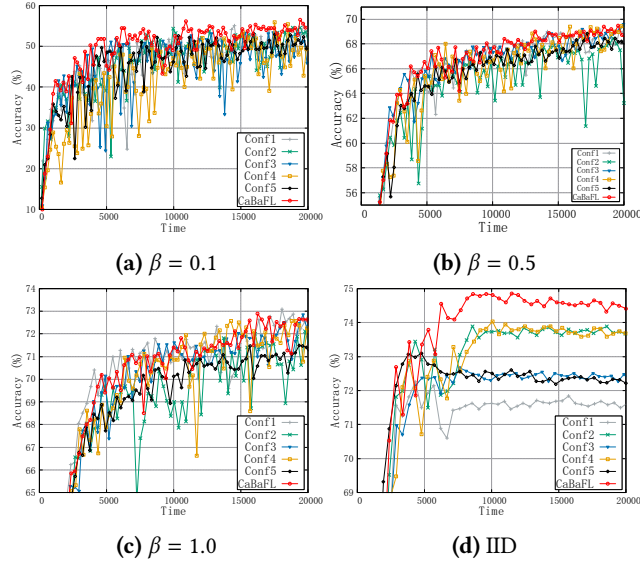


Figure 11. Ablation study results.

**5.4.2 Comparison of Activation and Hard Label.** In this section, we compare two different strategies for selecting devices based on activation (CaBaFL) and based on hard labels. Figure 12(a) and (b) shows the experimental results conducted on CIFAR-10 and ResNet-18 with IID distribution and Dirichlet distribution where  $\beta = 0.1$ . We can find that since the activation amount can represent the data distribution in a more fine-grained manner, selecting devices based on the activation can achieve better results in accuracy. Moreover, to demonstrate Observation 2, we design a special data distribution on CIFAR-100, i.e., the coarse-grained labels are balanced on each device, but the fine-grained labels are unbalanced. Figure 12(c) shows the experimental results conducted on ResNet-18. We can find that selecting devices based on activation performs better on training accuracy and stability. From the experimental results, we can conclude that our feature balance-guided device selection strategy can balance data in a more fine-grained manner compared to using hard labels.

## 5.5 Real Test-bed Evaluation

To demonstrate the effectiveness of our approach in physical environments, we conducted experiments on real devices using CNN models and the CIFAR-10 dataset considering both IID and non-IID ( $\beta = 1.0$ ) scenarios. We used an Ubuntu workstation equipped with an Intel i9 CPU, 32GB memory, and an NVIDIA RTX 3090Ti GPU as a server and used four NVIDIA Jetson Nano boards and six Raspberry Pi boards as heterogeneous clients. Our test-bed platform is shown in Figure 14. Figure 13 presents the learning curves of our CaBaFL and six SOTA FL methods on our test-bed platform. We can find that CaBaFL can also achieve the best performance compared to all the baselines. Please note that the

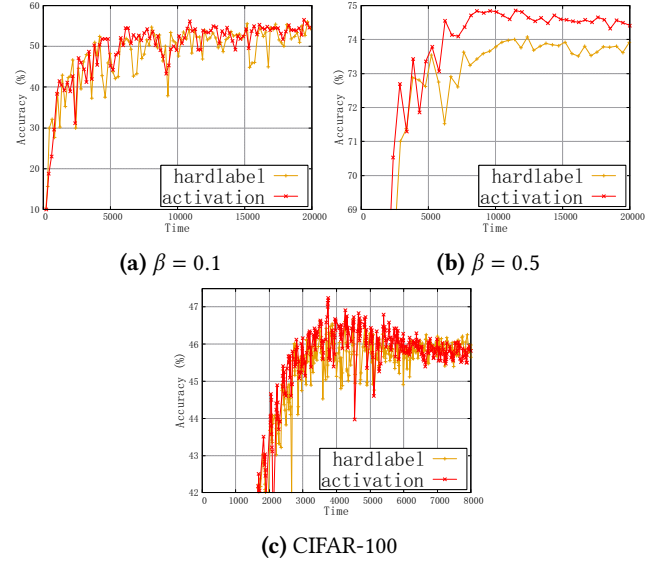


Figure 12. Comparison of activation and hard label.

number of samples per device in the real test-bed platform is much bigger than the number of samples per device in the simulation experiment. As a result, the experiment in Figure 11 is more likely to cause much more catastrophic forgetting even when  $\beta = 1.0$ , resulting in large amplitudes of the learning curves in Figure 13.

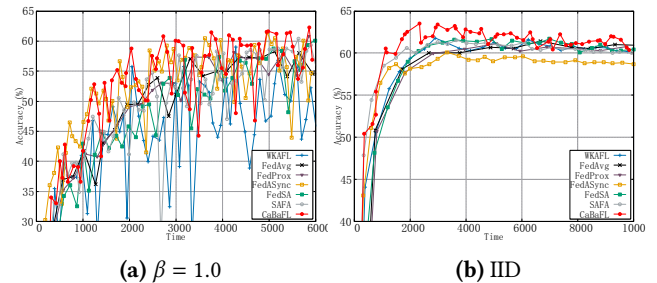


Figure 13. Learning curves on our test-bed platform.

## 5.6 Impact of Hyperparameters

To evaluate the impact of hyperparameters in CaBaFL, we set different configurations for  $\alpha$ ,  $\gamma$ , and  $\sigma$ , respectively, and performed experiments in the CIFAR-10 dataset using ResNet-18 model with IID and Non-IID ( $\beta = 0.1$ ) scenarios. Tables 7-9 exhibit the experiment results.

Table 7 shows the inference accuracy with different settings of  $\alpha$ . From Table 7, we can find that when the non-IID degree is high, a smaller  $\alpha$  can improve the accuracy of the model, while under the IID distribution, a larger  $\alpha$  can improve the accuracy of the model. This is mainly because when the degree of non-IID is high, the local data size of the

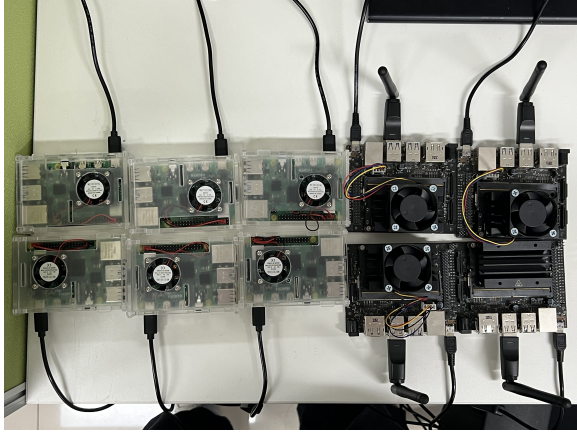


Figure 14. Our test-bed platform.

device varies greatly, so a smaller  $\alpha$  is needed to balance this difference, while the opposite is true in the case of IID.

Table 7. Impact of  $\alpha$  on test accuracy.

Hetero. Settings	Value of $\alpha$			
	0.5	0.7	0.9	1
$\beta = 0.1$	$55.46 \pm 0.67$	$54.63 \pm 0.46$	$55.14 \pm 0.79$	$53.70 \pm 0.79$
IID	$73.07 \pm 0.09$	$73.31 \pm 0.11$	$73.48 \pm 0.20$	$74.83 \pm 0.07$

Table 8 shows the impact of  $\sigma$ . We can find that when the non-IID degree is high, a larger  $\sigma$  can improve the accuracy of the model, while under the IID distribution, a smaller  $\sigma$  can improve the accuracy of the model. Please note that CaBaFL normalizes the number of times a device is selected before calculating the variance of the number of times the device is selected, so the value of  $\sigma$  is less than 0.

Table 8. Impact of  $\sigma$  on test accuracy.

Hetero. Settings	Value of $\sigma$			
	$1 \times 10^{-6}$	$2 \times 10^{-6}$	$3 \times 10^{-6}$	$4 \times 10^{-6}$
$\beta = 0.1$	$55.19 \pm 0.27$	$53.60 \pm 0.33$	$55.46 \pm 0.67$	$54.44 \pm 1.07$
IID	$74.83 \pm 0.07$	$72.80 \pm 0.10$	$73.17 \pm 0.15$	$73.72 \pm 0.09$

Table 9 shows the impact of  $\gamma$ . We can find that when the value of  $\gamma$  is appropriate, CaBaFL can achieve better global model accuracy. When the non-IID degree is high, a larger  $\gamma$ , i.e., filtering more models to make the cumulative training data of the model in L1 cache more balanced, is required to achieve higher global model accuracy, while under the IID distribution, a smaller  $\gamma$ , i.e., filtering few models, allows CaBaFL to achieve higher model accuracy.

Table 9. Impact of  $\gamma$  on test accuracy.

Hetero. Settings	Value of $\gamma$			
	0.4	0.3	0.2	0.01
$\beta = 0.1$	$54.59 \pm 1.62$	$55.56 \pm 0.77$	$54.08 \pm 1.04$	$53.26 \pm 1.95$
IID	$73.19 \pm 0.10$	$73.06 \pm 0.14$	$73.11 \pm 0.11$	$74.83 \pm 0.07$

## 6 Discussion

### 6.1 Fairness Issue

We have considered and addressed the fairness issues in CaBaFL using our device selection mechanism. In this mechanism, we use the hyperparameter  $\sigma$  to control the fairness of device selection. During the FL training, if the variance of the number of device selections exceeds  $\sigma$ , CaBaFL will select idle devices that have been touched least frequently, ensuring the fairness of device selection. We recorded the number of times a device was selected using our device selection strategy as well as the random selection strategy, and the results are shown in Figure 15. We can find that compared to the random selection strategy, except for a few outliers, the number of selected devices for our strategy is very close.

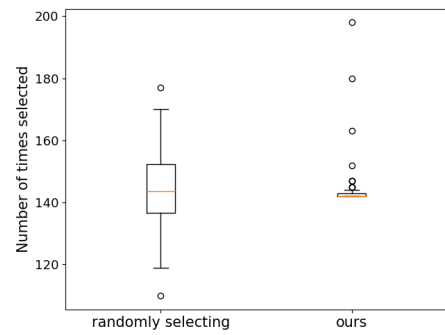


Figure 15. Comparison of random selection strategy and our feature balance-guided device selection strategy.

### 6.2 Complexity and Scalability

Our approach incurs negligible additional overhead in terms of time and memory, although our approach requires additional computation. Our approach thus has low complexity and high scalability even in large-scale AIoT environments. Next, we analyze the memory and time overhead separately.

In terms of memory cost, inspired by the concept of cache in the computer architecture domain, we developed a novel two-level cache-like data structure. Note that in implementing CaBaFL, we do not create a large memory space for the two-level cache. Instead, the cache design is implemented based on the indices of local models. Since the local models are also required to be collected by traditional FL methods and the sizes of indices are much smaller than the models, the memory overhead of our cache design is negligible.

In terms of time cost, assume that there are  $n$  devices involved in a  $k$ -round FL, and we are dealing with  $m$ -dimensional features, where  $k$  is the total number of interactions between devices and the server. For the whole FL, the complexity of cache update operations is  $O(km)$ , and the complexity of device selection is  $O(kmn)$ . Even for an FL system with 1000 devices, one round of cache update and device selection

costs less than 2ms, which is negligible compared with local training time.

### 6.3 Security Risks

In our method, the intermediate model is trained by different devices sequentially, meaning that the model produced by one device may be directly sent to another device. If an adversary can obtain the model updates produced by the former device, the adversary can figure out some privacy information. However, this situation is difficult to occur in our approach. This is mainly because the process of traversing devices by a specific intermediate model is controlled by the server based on our proposed device selection strategies. In this way, it is impossible for an adversary to figure out which device is a former one. Therefore, it is hard for the adversary to get the model updates.

### 6.4 Limitation

Our method makes it difficult to apply secure aggregation to protect privacy. Although there exist various privacy-preserving mechanisms (e.g. variational Bayes-based method), which can be easily integrated into our approach to secure the clients of CaBaFL, it also leads to a slight decrease in performance. Therefore, we need a better aggregation method that can perform secure aggregation without reducing accuracy.

In addition, there are a little too many hyperparameters in our method, and in the future, we may need an adaptive method to dynamically adjust these hyperparameters. We list these issues as our future work.

## 7 Conclusion

In this paper, we introduce CaBaFL, a new asynchronous federated learning mechanism. Firstly, CaBaFL effectively mitigates the straggler problem caused by device heterogeneity using the hierarchical cache-based aggregation mechanism. Secondly, CaBaFL enhances stability in its learning curve and global model accuracy by filtering models through a hierarchical cache. Thirdly, CaBaFL alleviates performance deterioration caused by data imbalance through the feature balance-guided device selection strategy. Experimental results demonstrate the efficacy of our proposed mechanism on datasets with both IID and varying degrees of non-IID.

In the future, we will figure out an algorithm to adaptively adjust the hyperparameters of our method. As another part of future work, we will also identify better aggregation methods to further protect privacy.

## References

- [1] Sebastian Caldas et al. 2018. *CoRR* abs/1812.01097 (2018). arXiv:1812.01097 <http://arxiv.org/abs/1812.01097>
- [2] Sebastian Caldas, Sai Meher Karthik Duddu, Peter Wu, Tian Li, Jakub Konečný, H Brendan McMahan, Virginia Smith, and Ameet Talwalkar. 2018. Leaf: A benchmark for federated settings. *arXiv preprint arXiv:1812.01097* (2018).
- [3] Cheng Chen, Ziyi Chen, Yi Zhou, and Bhavya Kailkhura. 2020. Fed-Cluster: Boosting the Convergence of Federated Learning via Cluster-Cycling. In *2020 IEEE International Conference on Big Data (Big Data)*. 5017–5026. <https://doi.org/10.1109/BigData50022.2020.9377960>
- [4] Yann Fraboni, Richard Vidal, Laetitia Kameni, and Marco Lorenzi. 2023. A general theory for federated optimization with asynchronous and heterogeneous clients updates. *Journal of Machine Learning Research* 24, 110 (2023), 1–43.
- [5] Avishek Ghosh, Jichan Chung, Dong Yin, and Kannan Ramchandran. 2022. An Efficient Framework for Clustered Federated Learning. *IEEE Transactions on Information Theory* 68, 12 (2022), 8076–8091. <https://doi.org/10.1109/TIT.2022.3192506>
- [6] Kaiming He, Xiangyu Zhang, Shaoqing Ren, and Jian Sun. 2016. Deep residual learning for image recognition. In *Proceedings of the IEEE conference on computer vision and pattern recognition*. 770–778.
- [7] Tzu-Ming Harry Hsu, Hang Qi, and Matthew Brown. 2019. Measuring the effects of non-identical data distribution for federated visual classification. *arXiv preprint arXiv:1909.06335* (2019).
- [8] Chung-Hsuan Hu, Zheng Chen, and Erik G Larsson. 2023. Scheduling and aggregation design for asynchronous federated learning over wireless networks. *IEEE Journal on Selected Areas in Communications* 41, 4 (2023), 874–886.
- [9] Ming Hu et al. 2023. AIoTML: A Unified Modeling Language for AIoT-Based Cyber-Physical Systems. *IEEE Transactions on Computer-Aided Design of Integrated Circuits and Systems (TCAD)* 40, 11 (2023), 3545–3558.
- [10] Ming Hu et al. 2024. FedMut: Generalized Federated Learning via Stochastic Mutation. In *Proceedings of the AAAI Conference on Artificial Intelligence*, Vol. 38. 12528–12537.
- [11] Husnoo et al. 2023. FeDiSa: A Semi-asynchronous Federated Learning Framework for Power System Fault and Cyberattack Discrimination. *arXiv preprint arXiv:2303.16956* (2023).
- [12] Jin et al. 2022. Personalized edge intelligence via federated self-knowledge distillation. *IEEE Transactions on Parallel and Distributed Systems* 34, 2 (2022), 567–580.
- [13] Peter Kairouz, H Brendan McMahan, Brendan Avent, Aurélien Bellet, Mehdi Bennis, Arjun Nitin Bhagoji, Kallista Bonawitz, Zachary Charles, Graham Cormode, Rachel Cummings, et al. 2021. Advances and open problems in federated learning. *Foundations and Trends® in Machine Learning* 14, 1–2 (2021), 1–210.
- [14] Sai Praneeth Karimireddy, Satyen Kale, Mehryar Mohri, Sashank Reddi, Sebastian Stich, and Ananda Theertha Suresh. 2020. SCAFFOLD: Stochastic controlled averaging for federated learning. In *Proceedings of International Conference on Machine Learning*. 5132–5143.
- [15] Sajad Khodadadian, Pranay Sharma, Gauri Joshi, and Siva Theja Maguluri. 2022. Federated reinforcement learning: Linear speedup under markovian sampling. In *International Conference on Machine Learning*. PMLR, 10997–11057.
- [16] Lingjing Kong, Tao Lin, Anastasia Koloskova, Martin Jaggi, and Sebastian Stich. 2021. Consensus control for decentralized deep learning. In *International Conference on Machine Learning*. PMLR, 5686–5696.
- [17] Alex Krizhevsky, Geoffrey Hinton, et al. 2009. Learning multiple layers of features from tiny images. (2009).
- [18] Alex Krizhevsky, Ilya Sutskever, and Geoffrey E Hinton. 2012. Imagenet classification with deep convolutional neural networks. *Advances in neural information processing systems* 25 (2012).
- [19] Lee et al. 2021. Adaptive transmission scheduling in wireless networks for asynchronous federated learning. *IEEE Journal on Selected Areas in Communications* 39, 12 (2021), 3673–3687.
- [20] Anran Li, Lan Zhang, Juntao Tan, Yaxuan Qin, Junhao Wang, and Xiang-Yang Li. 2021. Sample-level data selection for federated learning. In *IEEE INFOCOM 2021-IEEE Conference on Computer Communications*. IEEE, 1–10.

- [21] Tian Li, Anit Kumar Sahu, Ameet Talwalkar, and Virginia Smith. 2020. Federated learning: Challenges, methods, and future directions. *IEEE signal processing magazine* 37, 3 (2020), 50–60.
- [22] Tian Li, Anit Kumar Sahu, Manzil Zaheer, Maziar Sanjabi, Ameet Talwalkar, and Virginia Smith. 2020. Federated optimization in heterogeneous networks. *Proceedings of Machine learning and systems 2* (2020), 429–450.
- [23] Xiangru Lian, Wei Zhang, Ce Zhang, and Ji Liu. 2018. Asynchronous decentralized parallel stochastic gradient descent. In *International Conference on Machine Learning*. PMLR, 3043–3052.
- [24] Hui Lin, Kuljeet Kaur, Xiaoding Wang, Georges Kaddoum, Jia Hu, and Mohammad Mehdi Hassan. 2023. Privacy-Aware Access Control in IoT-Enabled Healthcare: A Federated Deep Learning Approach. *IEEE Internet of Things Journal* 10, 4 (2023), 2893–2902.
- [25] Liu et al. 2021. Feddgg: Federated domain generalization on medical image segmentation via episodic learning in continuous frequency space. In *Proceedings of the IEEE/CVF Conference on Computer Vision and Pattern Recognition*. 1013–1023.
- [26] Qianpiao Ma, Yang Xu, Hongli Xu, Zhida Jiang, Liusheng Huang, and He Huang. 2021. FedSA: A semi-asynchronous federated learning mechanism in heterogeneous edge computing. *IEEE Journal on Selected Areas in Communications* 39, 12 (2021), 3654–3672.
- [27] Brendan McMahan, Eider Moore, Daniel Ramage, Seth Hampson, and Blaise Aguera y Arcas. 2017. Communication-efficient learning of deep networks from decentralized data. In *Proceedings of Artificial intelligence and statistics*. 1273–1282.
- [28] Solmaz Niknam, Harpreet S Dhillon, and Jeffrey H Reed. 2020. Federated learning for wireless communications: Motivation, opportunities, and challenges. *IEEE Communications Magazine* 58, 6 (2020), 46–51.
- [29] Jihong Park, Sumudu Samarakoon, Mehdi Bennis, and M erouane Debah. 2019. Wireless network intelligence at the edge. *Proc. IEEE* 107, 11 (2019), 2204–2239.
- [30] Adam Paszke, Sam Gross, Francisco Massa, Adam Lerer, James Bradbury, Gregory Chanan, Trevor Killeen, Zeming Lin, Natalia Gimelshein, Luca Antiga, et al. 2019. Pytorch: An imperative style, high-performance deep learning library. *Advances in neural information processing systems* 32 (2019).
- [31] Sunitha Safavat and Danda B Rawat. 2023. Asynchronous Federated Learning for Intrusion Detection in Vehicular Cyber-Physical Systems. In *IEEE INFOCOM 2023-IEEE Conference on Computer Communications Workshops (INFOCOM WKSHPS)*. IEEE, 1–6.
- [32] Felix Sattler, Simon Wiedemann, Klaus-Robert M uller, and Wojciech Samek. 2020. Robust and Communication-Efficient Federated Learning From Non-i.i.d. Data. *IEEE Transactions on Neural Networks and Learning Systems* 31, 9 (2020), 3400–3413.
- [33] Donald Shenaj, Marco Toldo, Alberto Rigon, and Pietro Zanuttigh. 2023. Asynchronous Federated Continual Learning. In *Proceedings of the IEEE/CVF Conference on Computer Vision and Pattern Recognition*. 5054–5062.
- [34] Karen Simonyan and Andrew Zisserman. 2014. Very deep convolutional networks for large-scale image recognition. *arXiv preprint arXiv:1409.1556* (2014).
- [35] Chuan Sun, Xiuhua Li, Junhao Wen, Xiaofei Wang, Zhu Han, and Victor C. M. Leung. 2023. Federated Deep Reinforcement Learning for Recommendation-Enabled Edge Caching in Mobile Edge-Cloud Computing Networks. *IEEE Journal on Selected Areas in Communications* 41, 3 (2023), 690–705.
- [36] Wentai Wu, Ligang He, Weiwei Lin, Rui Mao, Carsten Maple, and Stephen Jarvis. 2020. SAFA: A semi-asynchronous protocol for fast federated learning with low overhead. *IEEE Trans. Comput.* 70, 5 (2020), 655–668.
- [37] Cong Xie, Sanmi Koyejo, and Indranil Gupta. 2019. Asynchronous federated optimization. *arXiv preprint arXiv:1903.03934* (2019).
- [38] Jinjun Xiong and Huamin Chen. 2020. Challenges for Building a Cloud Native Scalable and Trustable Multi-Tenant AIoT Platform. In *Proc. of International Conference on Computer-Aided Design (ICCAD)*.
- [39] Chenhao Xu, Youyang Qu, Yong Xiang, and Longxiang Gao. 2023. Asynchronous federated learning on heterogeneous devices: A survey. *Computer Science Review* 50 (2023), 100595.
- [40] Chen Yu, Hanlin Tang, Cedric Renggli, Simon Kassing, Ankit Singla, Dan Alistarh, Ce Zhang, and Ji Liu. 2019. Distributed learning over unreliable networks. In *International Conference on Machine Learning*. PMLR, 7202–7212.
- [41] Zhang et al. 2021. A survey on federated learning. *Knowledge-Based Systems* 216 (2021), 106775.
- [42] Zhang et al. 2023. FedMDS: An Efficient Model Discrepancy-Aware Semi-Asynchronous Clustered Federated Learning Framework. *IEEE Transactions on Parallel and Distributed Systems* 34, 3 (2023), 1007–1019.
- [43] Hongyi Zhang, Jan Bosch, and Helena Holmstr om Olsson. 2021. End-to-End Federated Learning for Autonomous Driving Vehicles. In *Proceedings of International Joint Conference on Neural Networks (IJCNN)*. 1–8.
- [44] Xinqian Zhang, Ming Hu, Jun Xia, Tongquan Wei, Mingsong Chen, and Shiyang Hu. 2020. Efficient federated learning for cloud-based AIoT applications. *IEEE Transactions on Computer-Aided Design of Integrated Circuits and Systems* 40, 11 (2020), 2211–2223.
- [45] Zhao Zhang, Yong Zhang, Da Guo, Shuang Zhao, and Xiaolin Zhu. 2023. Communication-efficient federated continual learning for distributed learning system with Non-IID data. *Science China Information Sciences* 66, 2 (2023), 122102.
- [46] Zihao Zhou, Yanan Li, Xuebin Ren, and Shusen Yang. 2022. Towards Efficient and Stable K-Asynchronous Federated Learning with Unbounded Stale Gradients on Non-IID Data. *IEEE Transactions on Parallel and Distributed Systems* 33, 12 (2022), 3291–3305.